

ULTRASONIC FATIGUE ANALYSIS ON AN AUSTENITIC STEEL AT HIGH TEMPERATURE

Federico Cavalieri^{a,b}, Claude Bathias^b, Nicolas Ranc^b, Alberto Cardona^a and José Risso^a

^a*Centro Internacional de Métodos Computacionales en Ingeniería (CIMEC-INTEC). CONICET - Universidad Nacional del Litoral*

Güemes 3450, (3000) Santa Fe, Argentina, fcavalieri@ceride.gov.ar <http://www.cimec.org.ar>

^b*Laboratoire d'Énergetique et d'Économie d'Énergie Université - Paris X*

Rue de Sévres, 92410 Ville d'Avray, Paris, France, claude@bathias.com <http://www.cba.u-paris10.fr>

Keywords: Fatigue, high cycles number, high temperature, austenitic steel, finite element method.

Abstract. In this work, an ultrasonic fatigue technique is presented to study the fatigue behavior on an austenitic steel at high temperatures under fully reverse loading ($R=-1$) in the lifetime range from 10^5 to 10^9 cycles. This material is employed in internal combustion engine valves. To carry out the fatigue tests at high temperatures, an induction coil heating equipment was employed to achieve temperatures as high as 600°C and 700°C on the specimens. Since Young modulus is a function of temperature, its value changes when the specimen is heated. We analyzed with a numerical methodology (finite element method, FEM), the effects of the variation in the Young modulus due to temperature from the measurement of the ultrasonic resonance frequency. Thermal, thermo-mechanical and modal analysis by FEM was used for designing the specimens at test temperatures. The commercial software was employed for the numerical simulations.

1 INTRODUCTION

One of the main catastrophic causes of failure in internal combustion engine valves is fatigue. Mechanical stresses in valves are generated by loads coming from the return spring, the inertia loads of retainer, keeper and stem and the thermal loads from the combustion. Usually, stresses are developed in the axial direction of the stem, produced by the impact between the valve head and the valve seat during the closing cycles. Stress propagates through the stem and can lead ultimately to a fatigue failure. Nowadays, many car engine valves require an operative life beyond 10^8 cycles, being necessary to investigate the fatigue behavior of valve materials in the gigacycle range to improve their design. Using classical fatigue criterions, a near hyperbolic relationship between stress and fatigue life is assumed, but experimental results show that the fatigue fracture can occur beyond 10^7 cycles and the concept of endurance limit is not correct (Bathias et al., 2001). Numerous works have shown that the fatigue behavior of different kinds of materials (Bathias and Paris, 2005; Mayer, 2003; Willertz, 1980) in the gigacycle regime can be obtained effectively by using ultrasonic fatigue testing machines, and that frequency effects are not important in the determination of the lifetime. Many studies in this field have been reported at room temperature (Marines et al., 1999; Bayraktar et al., 2006; Zettl et al., 2006), but available database information at high temperature is very scarce, because the time to reach 10^9 cycles at high temperature using traditional low cycle fatigue testing machines is an almost impossible task to perform. Under these conditions, ultrasonic fatigue testing is a new attractive technique which allows us to get fatigue results in a shorter time and with lower costs compared to traditional fatigue procedures. In this work, we present a methodology to get mechanical and fatigue properties of an austenitic steel of engine valves subjected to very high cycle loadings ($R=-1$) at high temperatures employing the ultrasonic fatigue testing machine and numerical simulations.

The fatigue machine used in this work has a nominal frequency of 20 kHz obtaining 10^9 cycles in approximately 14 hours. A specially design induction coil was used for specimen heating to achieve temperatures of 600°C and 700°C, with constant temperature profile in the gage section of the specimen and an intrinsic resonance frequency close to 20kHz for each temperature tested. The fracture surface in the broken specimens was inspected using both optical and Scanning Electronic (SEM) Microscopy.

The numerical simulation by FEM was used for designing the specimen at both room and high temperatures. There was no previous information about the mechanical properties of this material in ultrasonic regime at high temperatures, which are imperative for its design and to obtain the fatigue curve stress (S) vs. cycles numbers (N). Thus, a cylindrical specimen was tested at high temperature on the gigacycle fatigue testing machine measuring its resonance frequency. Then, once the temperature distribution is known, a finite element axisymmetric specimen model was developed using an inverse method described in Sec. 5 in order to determine the dynamic Young modulus as a function of temperature. The analyses by FEM were: thermal, thermo-mechanical and modal. Thermal analyses were used to know temperature distribution along the length of the specimen, thermo-mechanical analysis to know the specimen thermal expansion, displacement and stress fields and a modal analysis to modify the design of the specimen in order to get a natural frequency close to 20kHz at high temperature.

Finally, fatigue curves S-N at 20°C, 600°C and 700°C are provided in Sec. 7 with the discussion about the results obtained.

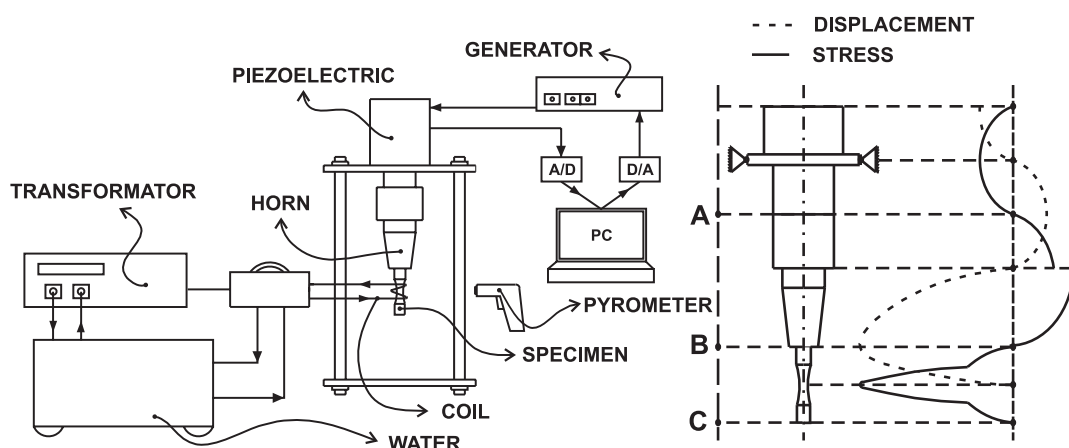


Figure 1: Fatigue testing machine and vibratory stress and displacement field.

2 TENSION-COMPRESSION PIEZOELECTRIC FATIGUE MACHINE

The first ultrasonic fatigue testing machine was introduced by Mason [W.P \(1950\)](#). In the last two decades research advances in this area have been very important. At Institute for Technology and Advanced Materials (ITMA), the ultrasonic fatigue technique capabilities have been extended to torsional, high and low temperatures and fretting analysis tests ([C., 2006](#); [Sun et al., 2001](#)). In this work, we have used an ultrasonic fatigue testing machine and the procedures from ITMA to carry out ultrasonic fatigue tests at high temperatures on austenitic steel. There are many designs of ultrasonic machines but they always have three main components, (see figure 1):

1. An electric power generator which converts 60 Hz voltage into an electrical sinusoidal signal.
2. A piezoelectric transducer which transforms the electrical signal into mechanical vibration of the same frequency.
3. An ultrasonic horn that amplifies the vibration coming from the transducer in order to obtain the required stress amplitude in the middle section of the specimen.

The generator is connected to a PC and it is associated to an acquisition card A/D and D/A for controlling the generator and the piezoelectric actuator that induced the mechanical movement. The transducer generates a mechanical wave with an intrinsic frequency of 20 kHz and for this reason, the specimen must be designed with this same natural frequency in its first mode of vibration, reaching a maximum displacement (null stress) at the end and maximum stress (null displacement) in the central section as, it is shown in figure 1.

The machine is used for fatigue life analysis at more than 10^5 cycles, because with lower values plastic phenomena appears and thus, a low cycle fatigue testing machine would be suitable. The operative frequency range is from 19.5 to 20.5 kHz and if it decreases below to 19.5 kHz or increases up to 20.5 kHz, the test is stopped automatically. All the stresses and displacements are linear, being only necessary to measure the displacement amplitude to compute the stresses. In contrast with the low cycle fatigue tests, where the machine has a natural frequency different from the specimen, in the ultrasonic fatigue machines, the specimen-machine conforms a resonance system in which the displacement amplitudes are kept constant during the test at a pre-selected value. In addition to the main components of an ultrasonic fatigue machine, some

additional devices can be used, as shown in figure 1. The basic components of the induction equipment for specimen heating and a measuring instrument (infra red pyrometer) to control the temperature are schematically shown in the figure 1. A more detailed explanation about the ultrasonic fatigue testing machine is presented in C. (2002); Bathias and Paris (2005).

3 MATERIAL

The material used in this research is an austenitic steel widely used in internal combustion engine valves due to its high strength, small Young modulus variation at high temperatures and good resistance to oxidation. The chemical composition is shown in table 1 and the mechanical properties in table 2. Since Young modulus and density are the dominant variables in ultrasonic tests, it is very important to know their values as accurate as possible. The density ρ and the static Young modulus E_{static} at room temperature are 7.7g/cm^3 and 215×10^3 MPa respectively. The dynamic Young modulus at different temperatures was determined following the procedure presented in Sec. 5.

Steel	C	Si	Mn	Cr	Ni	W	Nb	N
H854	0.53	0.25	9.5	21	3.8	1	2.2	0.5

Table 1: Chemical composition of the analyzed steel.

Steel	ρ [g/cm ³]	E_{static} [N/mm ²]	UTS [N/mm ²]	T. Conductivity at 20°C [W/m.K]	T. Expansion at 500°C [m/m.K]
H854	7.7	215×10^3	950 – 1150	14.5	18.8

Table 2: Thermo mechanical properties of the analyzed steel.

Figure 2 shows a general view of the microstructure obtained with an optic microscope, where it is possible to see the austenitic structure.

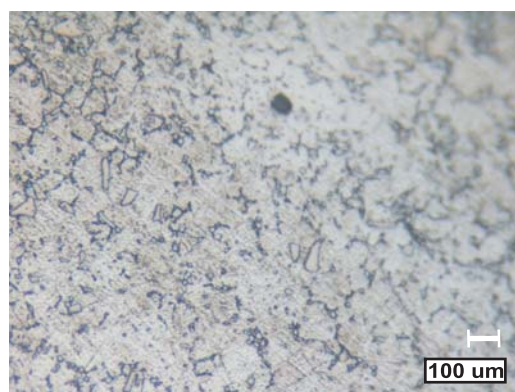


Figure 2: Austenitic microstructure of the analyzed material.

4 ANALYTICAL AND NUMERICAL MODELS FOR DESIGNING A SPECIMEN

The ultrasonic fatigue principle is easy to show through a simple mathematical model with two masses m vibrating and linked by a spring of stiffness k . It follows that resonant frequency

is given by,

$$f_{\text{reso}} = \frac{1}{2\pi} \sqrt{\frac{k}{m}} \tag{1}$$

It is important to note that at the ends, where the masses are located, the displacements are maximum, and in the middle of the spring, the displacement is null. This system is a simple discrete model which gives us a first conceptual idea about how the vibration frequency of an ultrasonic specimen should be. However, using a continuum model, it is possible to obtain a more accurately representation, for instance, taking a bar and neglecting the transversal contraction, the frequency is given by:

$$f_{\text{reso}} = \frac{1}{2L} \sqrt{\frac{E_d}{\rho}} \tag{2}$$

where E_d is the dynamic Young modulus which considers the dynamics effects and it is usually different from static Young modulus, ρ the density and L the bar length.

4.1 Specimen design for room temperature

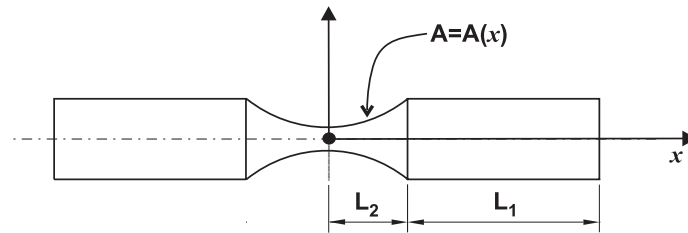


Figure 3: Ultrasonic specimen geometry.

In a general specimen geometry, see figure 3, the transversal section has a variation along the length and for this reason equation (2) can not be used. However, a better representation of the displacement, strain and stress are obtained from analytical expressions (Bathias and Paris, 2005) which solve the following ordinary differential equations system:

$$\begin{cases} U_r''(x) + U_r' \left(\frac{A'(x)}{A(x)} \right) + \frac{\omega^2 \rho}{E_d} U_r(x) = 0 \\ U_c''(x) + U_c' + \frac{\omega^2 \rho}{E_d} U_c(x) = 0 \\ U_r(L_2) = U_c(L_2) \\ U_c'(L) = 0 \\ U_c(L_2) = B_0 \\ U_r(0) = 0 \end{cases} \tag{3}$$

where x corresponds to the longitudinal coordinate, $A(x)$ is the cross section, L_2 is gage length of the specimen, L_1 is the cylindrical or resonance length, $L = L_1 + L_2$, E_d is the dynamic Young modulus and B_0 is an imposed displacement. There, $U_c(x)$ is the displacement field in the cylindrical section, $L_2 < |x| \leq L$ and $U_r(x)$ corresponds to the displacement filed in the gage section, $|x| \leq L_2$. We are mainly interested in the determination as accurately as possible of the maximum stress in the middle of the specimen with a resonance frequency of 20kHz in its first vibration mode. A modal analysis with an axisymmetric FEM model was also performed using SAMCEF (2007). The geometry used in the FEM model was initially obtained

from the analytical expressions equation 3 and later it was modified by changing the specimen length for obtaining a resonant frequency of 20kHz. Experimental results on gigacycle testing machine showed that the designed specimen vibrated with a natural frequency of 19.98kHz. Final dimensions of the specimen for room temperature are shown in figure 4. Then, the stress and displacement fields were computed using both FEM mechanical analysis and analytical equations. To carry out the mechanical analysis, an initial position and a prescribed position variable in time with a frequency of 20 kHz were imposed in the FEM model as it is shown in figure 7. The dynamic Young modulus and the density values were those for room temperature. Since the displacement solutions are anti-symmetric and the stress solutions are symmetric, only one half of the displacement and stress distribution in the specimen was determined. A comparison between the FEM and the analytic solution of the displacements and stresses is shown in figure 5.

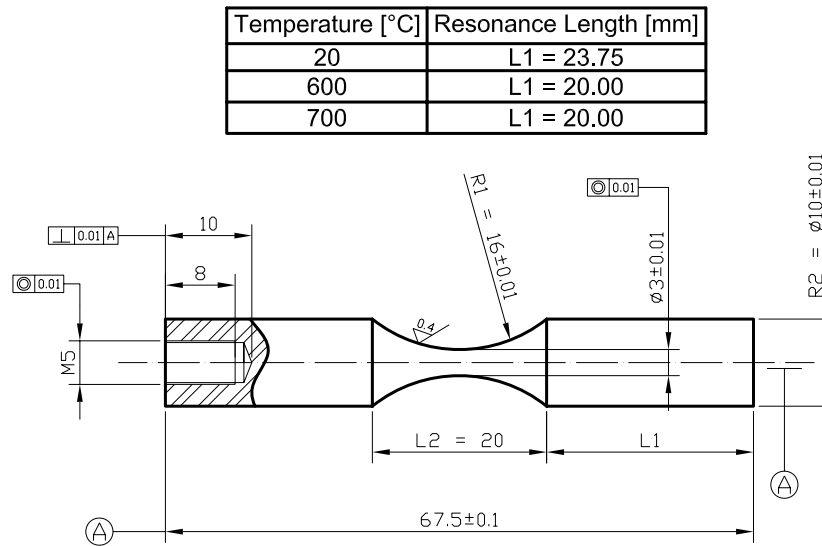


Figure 4: Boundary conditions and thermal and modal FEM solutions for the cylindrical specimen.

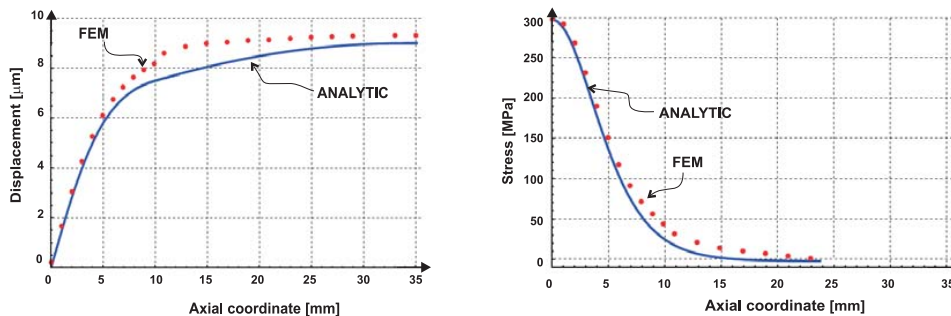


Figure 5: Displacement and Stress comparison between the analytic and FEM methods for 20°C.

4.2 Specimen design at high temperature

When a specimen is heated at high temperature, the resonant frequency is affected by geometric changes and the decrease of the Young modulus produced by the thermal effects. For

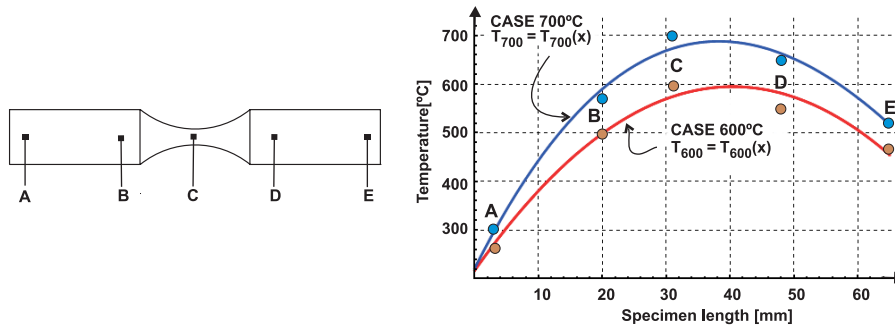


Figure 6: Temperature measured points on non cylindrical specimen.

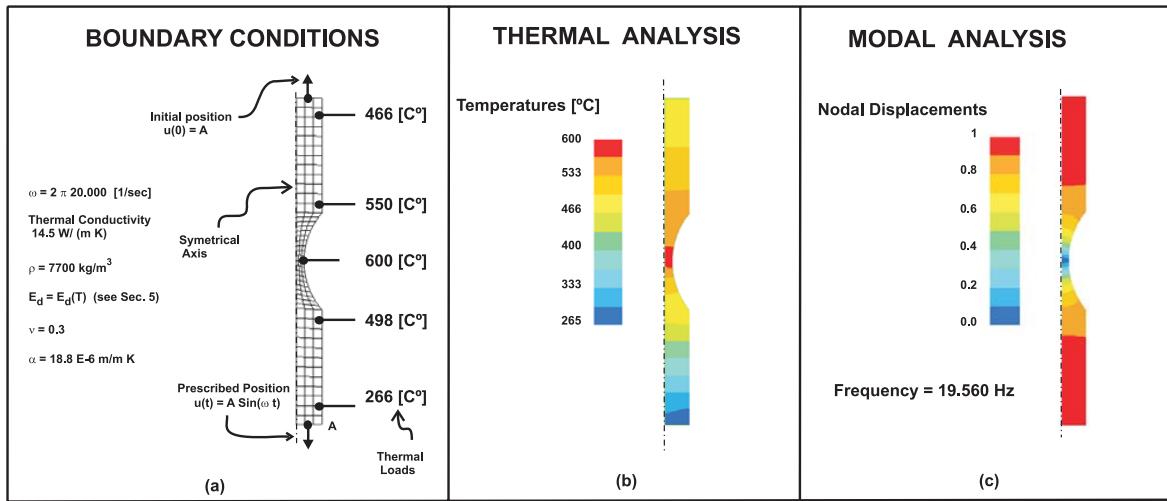


Figure 7: Thermal and modal analysis of the specimen at 600°C by FEM.

this reason, it is necessary to modify the specimen geometry in order to achieve a natural frequency as close as possible to 20 kHz at the desired temperature. In other words, the resonance frequency of the specimens used at high temperature should be shorter than those used for room temperature Shyam et al. (2004); Yi et al. (2007). As a result of the heating, dynamic Young modulus is position depending in the specimen when it is heated, $E_d = E_d(x)$, and for this reason, analytic solutions are not longer valid to solve (4). Thus, in order to design a specimen for high temperature tests, first we have used an axysimmetric FEM analysis and then, the solutions were compared with those obtained by solving numerically (4).

$$\begin{cases}
 U_r''(x) + U_r' \left(\frac{A'(x)}{A(x)} + \frac{E_d'(x)}{E_d(x)} \right) + \frac{\omega^2 \rho}{E_d(x)} U_r(x) = 0 \\
 U_c''(x) + U_c' \left(\frac{E'(x)}{E_d(x)} \right) + \frac{\omega^2 \rho}{E_d(x)} U_c(x) = 0 \\
 U_r(L_2) = U_c(L_2) \\
 U_c'(L) = 0 \\
 U_c(L_2) = B_0 \\
 U_r(0) = 0
 \end{cases} \quad (4)$$

4.2.1 Design by FEM.

The temperature variation along the specimen was determined experimentally with a specimen whose dimensions were not the definitive ones. The experimentally measured temperatures, see figure 6, were introduced into an axisymmetric FEM model as thermal loads as shown in figure 7 for the case of 600°C. The temperature distribution was given by a thermal calculation with an initial specimen geometry computed for room temperature tests. Dynamic Young modulus is included as variable with the temperature to perform a thermo mechanical and modal analysis. Finally, with a geometry modified by the thermal effects, the modal analysis is conducted for obtaining the resonant frequency. If this frequency was not close to 20 kHz, the length of the specimen should be modified. This procedure was repeated two or three times until a satisfactory frequency response was found. Final dimensions of the specimens for the temperature cases of 600°C and 700°C are shown in figure 4.

In order to obtain the stress and displacements, a thermo-mechanical analysis was performed with the boundary conditions shown in figure 7. Displacements and stress FEM solutions for the temperature cases of 600°C and 700°C are shown in figures 8 and 9.

4.2.2 Design by RK4 integration method

The displacements and stresses fields obtained previously by FEM are compared with the numerical solutions of (4) given by Runge Kutta - (RK4) method. For that, it is necessary to know the dynamic Young modulus variation along the length of the specimen, $E_d = E_d(x)$. Using the experimental temperature distribution $T_{600} = T_{600}(x)$ and $T_{700} = T_{700}(x)$, for each temperature cases (see figure 6), and the Young modulus as a function of the temperature $E_d = E_d(T)$ (calculated in Sec. 5), the relationship $E_d = E_d(T(x))$ is established. The comparison of the displacements and stress solutions between FEM and RK4 for the cases of 600°C and 700°C are plotted in figures 8 and 9 respectively. Solutions of both methods showed good agreement.

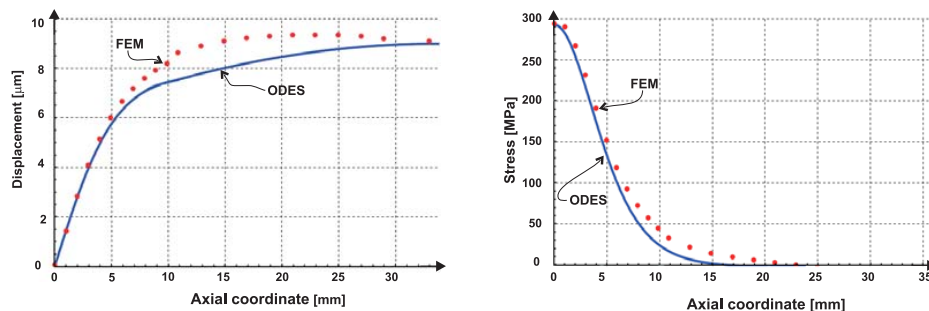


Figure 8: Displacement and Stress comparison between the RK4 and FEM methods for 600°C.

5 EXPERIMENTAL PROCEDURE FOR DYNAMIC YOUNG MODULUS DETERMINATION

In Sec. 4, dynamic Young modulus E_d was presented as a mechanical characteristic which considers the dynamics effects during ultrasonic fatigue testing, so the relationship between E_d and the temperature $E_d = E_d(T)$ is required for designing a specimen in an ultrasonic load regime at high temperature. Mechanical properties database for the material presented in this work is very scarce and consequently, new experimental tests were the only way to get the relationship $E_d = E_d(T)$. Thus, first we have studied the Young modulus influence with the

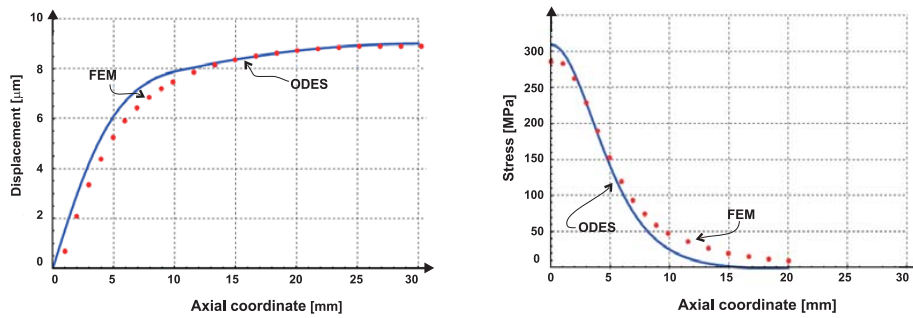


Figure 9: Displacement and Stress comparison between the RK4 and FEM methods for 700°C.

resonant frequency of a cylindrical specimen at room temperature and later at high temperature, using the gigacycle fatigue testing machine and numerical simulations by FEM.

5.1 Dynamic Young modulus at room temperature

In order to determine E_d at room temperature, a cylindrical specimen initially of length L was designed using equation (2) as $L = (2f_{reso})^{-1}(E_{static}/\rho)^{0.5}$ with the static Young modulus, from table 2, and a resonance frequency $f_{reso} = 20$ kHz. Since the measured frequency was lower than 20 kHz, the specimen was cut until measuring experimentally f_{reso} . Final dimensions of the specimen are shown in figure 10. The dynamic Young modulus was obtained as $E_d = \rho(2L 20.000)^2$, see figure 12(b).

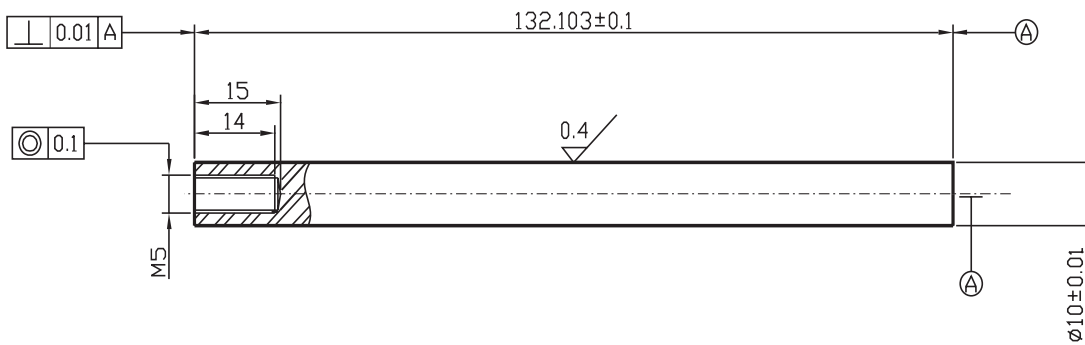


Figure 10: Cylindrical specimen dimensions.

5.2 Dynamic Young modulus at high temperature

An induction coil was used for heating the cylindrical specimen shown in figure 10. A scheme of the heating equipment setup used in this work is shown in figure 1. Temperature was measured with an optical pyrometer as well as with thermocouples connected along the length of the specimen. Six tests were conducted, registering the temperatures in different points of the specimen and the resonance frequency as shown in table 3. Where L_i is the length from the top of the specimen to the measured point, see figure 11. The maximum temperature is located in the point L_3 . At high temperature, the procedure used the previous section, based in equation (2) is not longer valid, and the task to determine an accurate variation of E_d with temperature is more difficult.

As Young modulus is a function of the temperature, it changes its value from point to point. Furthermore, one specimen end is refrigerated to avoid a big dilatation in the connection with

CASE	I	II	III	IV	V	VI	VI
$L_1 = 15$ [mm]	20°C	53°C	100°C	96°C	130°C	150°C	210°C
$L_2 = 32$ [mm]	20°C	76°C	152°C	200°C	240°C	330°C	420°C
$L_3 = 64$ [mm]	20°C	100°C	200°C	300°C	400°C	500°C	550°C
$L_4 = 94$ [mm]	20°C	80°C	155°C	250°C	340°C	430°C	500°C
$L_5 = 113$ [mm]	20°C	65°C	130°C	200°C	300°C	380°C	400°C
Frequency [kHz]	19.98	19.89	19.82	19.73	19.64	19.54	19.50

Table 3: Temperature and frequency values measured on cylindrical specimen.

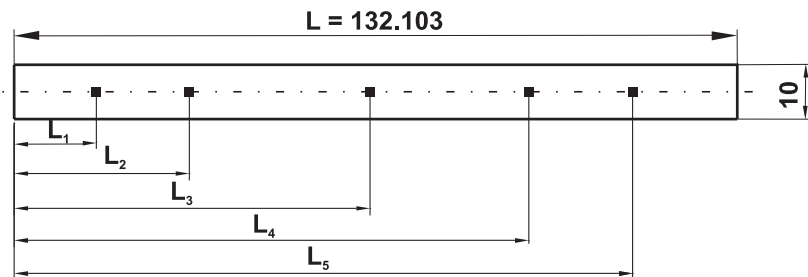
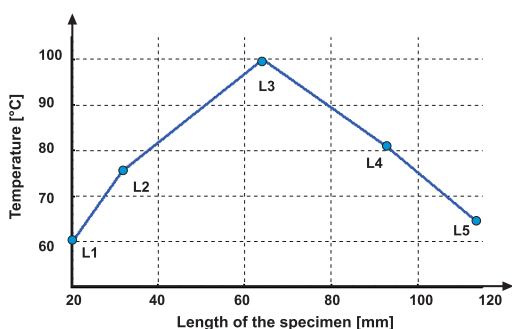


Figure 11: Temperature measured points on cylindrical specimen.

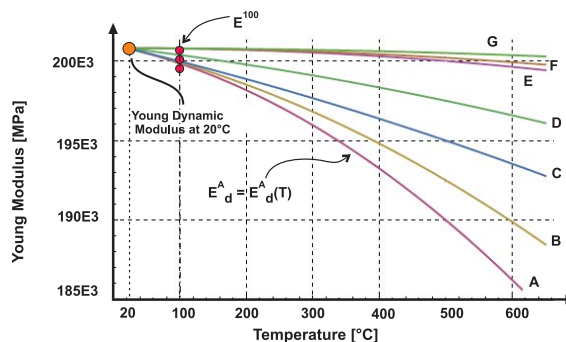
the horn, thus temperature distribution is neither constant along the length nor symmetrical about the middle section. In this work, an inverse method to obtain $E_d = E_d(T)$ from the measurement of ultrasonic resonance frequency and FEM is presented. We begin by performing a FEM thermal analysis with the measured temperatures at each point as Dirichlet or essential boundary conditions, as is shown for instance in figure 12(a) for case II, determining thermal expansion and temperature distribution. The computed temperature distribution is entered as data for a FEM modal analysis and the variation of E_d according to one of the proposed laws $E_d = E_d^j(T)$, $j=A,B,\dots,G$, plotted in figure 12(b). Then, for each case, i ($i=I,\dots,VI$), a resonance frequency f_{reso}^{ij} is numerically computed for the E_d^j law.

In figures 13(a), 13(b) and 13(c) are shown the FEM boundary conditions and the solutions of the thermal and modal analysis for the case II respectively.

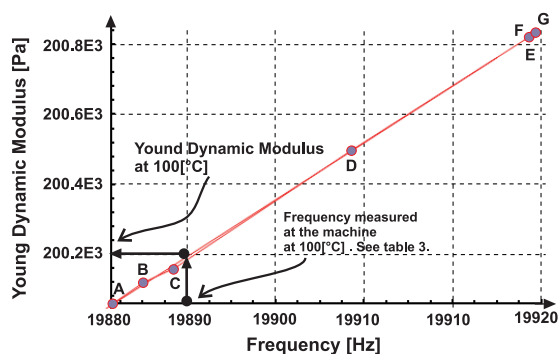
Now, let us adopt a temperature value T_i as characteristic of the case i , for instance, the maximum temperature. A list like that represented in figure 12(c) for case II is built, where the numerically computed frequencies are the abscissa and the values of E_d for T_i are the ordinates. The final value of E_d we will adopt for T_i is that corresponding to the measured frequency f_{measured} , obtained by linear interpolation between the closest frequency values. Repeating this procedure for the remainder cases, the relationship $E_d = E_d(T)$ plotted in figure 12(d) is obtained.



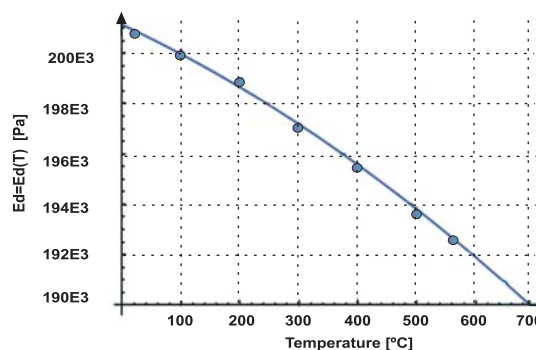
(a) Temperature distribution for case II.



(b) Family curves of $E_d = E_d(T)$.



(c) E_d vs. f_{reso} for case II.



(d) Young Dynamics Modulus vs. Temperature for the steel analyzed.

Figure 12: Numerical methodology to obtain the relationship $E_d = E_d(T)$.

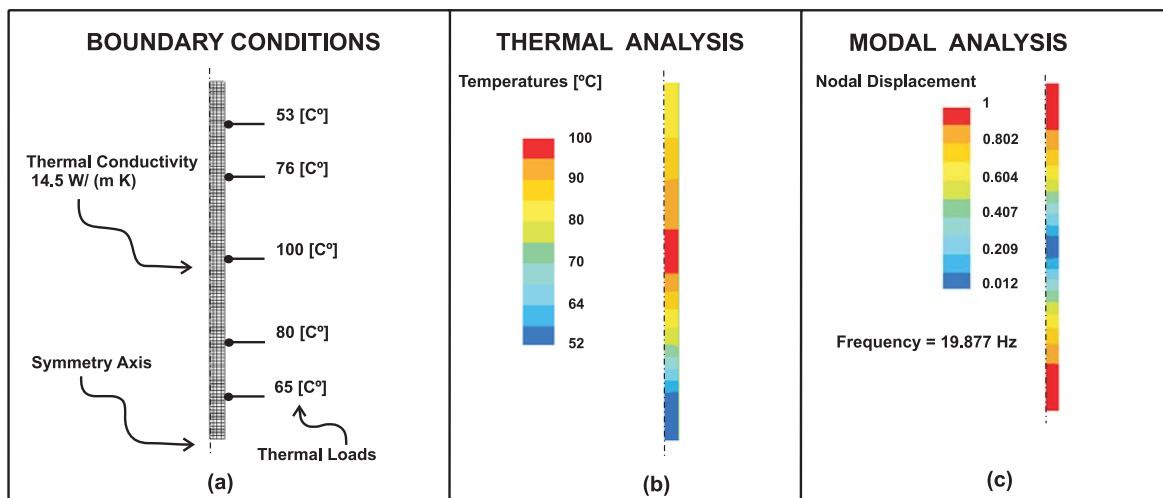


Figure 13: Boundary conditions, thermal and modal solutions for the temperature case II.

6 EXPERIMENTAL PROCEDURE FOR FATIGUE TESTS

In the tests at high temperatures, an induction coil technique was used as previously mentioned. The coil was made of a copper tube with a spiral shape situated in the middle of the specimen and designed from (Curtis, 1950), to heat the specimen around its middle section. An optical pyrometer was used during the tests to measure and control temperature at the center of the specimen. Its emissivity was calibrated with a reference instrument. The correct emissivity was found when both instruments detected the same temperature. Thermocouples have been also used to calibrate the pyrometer and to measure the temperature during the tests. The pyrometer presents some practical advantages compared to the thermocouple, because it does not require any welding to the specimen, allowing measurements in different points in a very easy way. The temperature elevation of the material due to ultrasonic loadings was studied with an infrared camera. In Sec. 7.1, (see figure 17) there are some comments about this effect.

The ultrasonic fatigue testing machine calibration is required to make the system vibrate in resonance at ultrasonic frequency of about 20 kHz. It has been performed with a cylindrical specimen and an optic fiber sensor situated at one specimen end, which registers displacements from $1\mu\text{m}$ to $199.9\mu\text{m}$ with a resolution of $0.1\mu\text{m}$. This calibration was also checked with the software of the testing machine.

The mechanical system works in an elastic regime and consequently the relationships between displacement, strain and stress are linear. In the machine used in this work, the electrical voltage is also linear and proportional to the displacement. Figure 14 shows a comparison of the displacement and voltage, measured with the optical sensor and the computer software. Finally, the stress amplification factor for obtaining the stress in the specimen by the analytical calculation, is obtained using these measurements. First, room temperature fatigue tests have

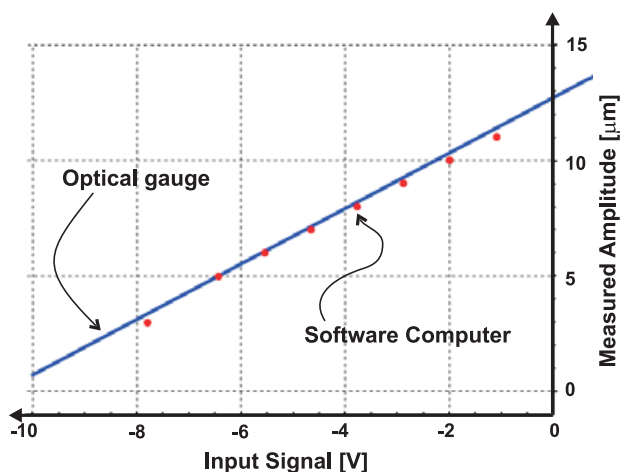


Figure 14: Measured amplitude of signal.

been performed, and then in a similar way but incorporating thermal effects, at temperatures of 600°C and 700°C . Specimens geometry used for each test was shown in figure 4.

Specimens which did not fail beyond 10^9 cycles, were considered runouts and incremental stress was applied to them until obtaining the fatigue rupture. Geometry and resonance frequency of 20 kHz were checked in the specimens before starting each test, and a maximum tolerance of ± 200 Hz was established as a variation range for the frequency. In the tests, the machine stopped automatically when a crack propagated rapidly causing a change in the resonance frequency of the system. The S-N curves obtained for the tests are shown in Sec. 7.

7 EXPERIMENTAL RESULTS AND DISCUSSIONS

7.1 S-N curve at Room Temperature

The stress life response of the material tested at room temperature is shown in figure 15 in a semi-log plot. ? defined the endurance limit as the range of cyclic stress that can be applied to

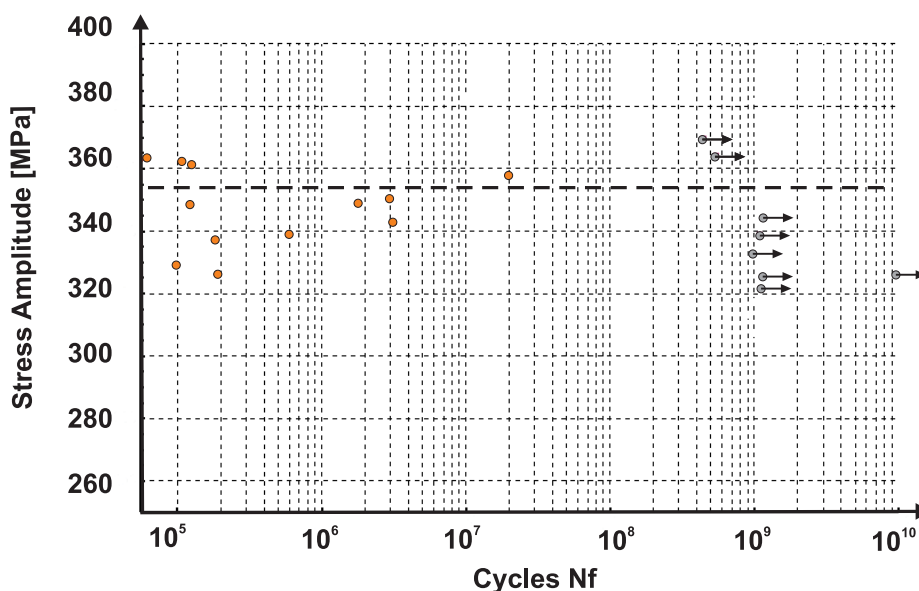
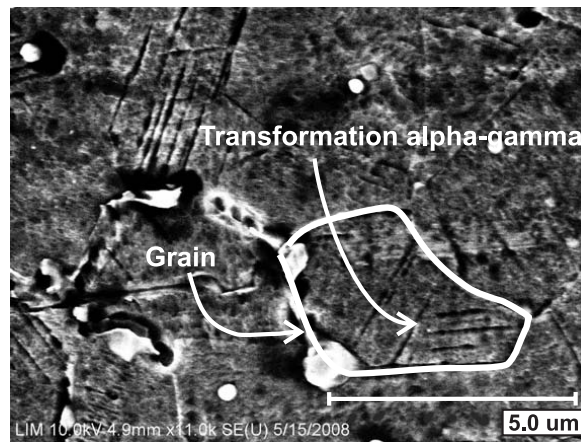


Figure 15: S-N curve at room temperature for the material analyzed.

the material without causing fatigue failure. In this material the dashed line shows the endurance limit with a value of about 353 MPa. The arrows in the S-N plot, indicate that the specimens did not fail up to 10^9 cycles (runouts).

All cracks were initiated at a surface location and no interior crack initiations from inclusions were found. The highest cycles number for a failed specimen was 2×10^7 cycles. In the specimens which run until 10^9 cycles, the resonant frequency did not decrease during the tests, indicating that there was no crack initiation. SEM inspection has been performed on fatigue specimen fracture surfaces, showed that there were microstructural changes during the tests. In the original state, the material has an austenitic microstructure, (figure 2), but with few cycles of loading, a microstructural transformation to martensite is developed. The SEM image of figure 16(a) shows the $\alpha - \gamma$ martensite lines inside the grains in a specimen which runs out up to 10^9 cycles. Furthermore, a temperature variation measured during the tests confirmed that some kind of transformation occurs. Figure 17 shows the temperature increment due to the microstructural transformation and the cyclic plastic deformation, registered by an infrared red camera during the tests. The maximum temperature without cooling was 280°C , decreasing to a value of 240°C after 10^7 cycles. In order to reduce this problem as much as possible, maximum cooling in the middle of the specimen was used reaching a temperature of about 150°C .

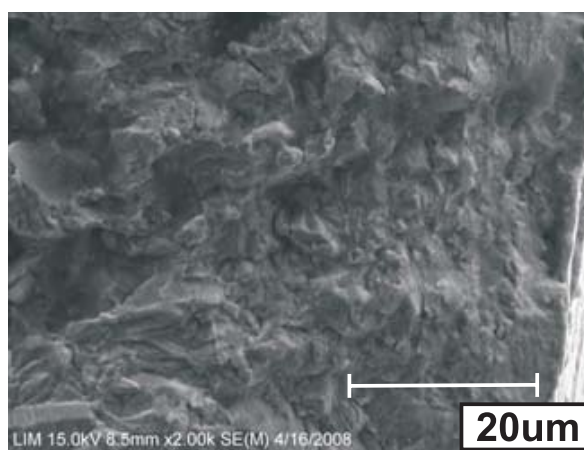
According to the research of [Marines et al. \(1999\)](#), the fatigue strength is sensitive to the specimen surface finishing for fatigue tests in the gigacycle regime at room temperature. Surface roughness could generate a stress concentration contributing to accelerate the fatigue damage. Figure 16(b) shows the fracture surface of a specimen failed at 337 MPa with a lifetime of 1.85×10^5 cycles using an optical microscope. The rupture surface was normal to the longitudinal axis



(a) Microstructural Transformation α - γ .



(b) Fracture surface of the specimen failed at 337MPa in 1.85×10^5 cycles at 20°C.



(c) Fracture surface of the specimen failed at 337MPa in 1.85×10^5 cycles at 20°C.

Figure 16: Microstructural Transformation and Fracture Surfaces in a specimen at 20°C.

in the middle of the specimen. The blue color represents the maximum temperature before the final crack. Figure 16(c), obtained using SEM, shows some striation formation on the fracture surface on a specimen which failed at 1.85×10^5 cycles at 337MPa. Finally, we concluded that the microstructural transformation and the influence of stress concentration due to surface roughness are the main causes to explain the premature failure of some specimens at room temperature.

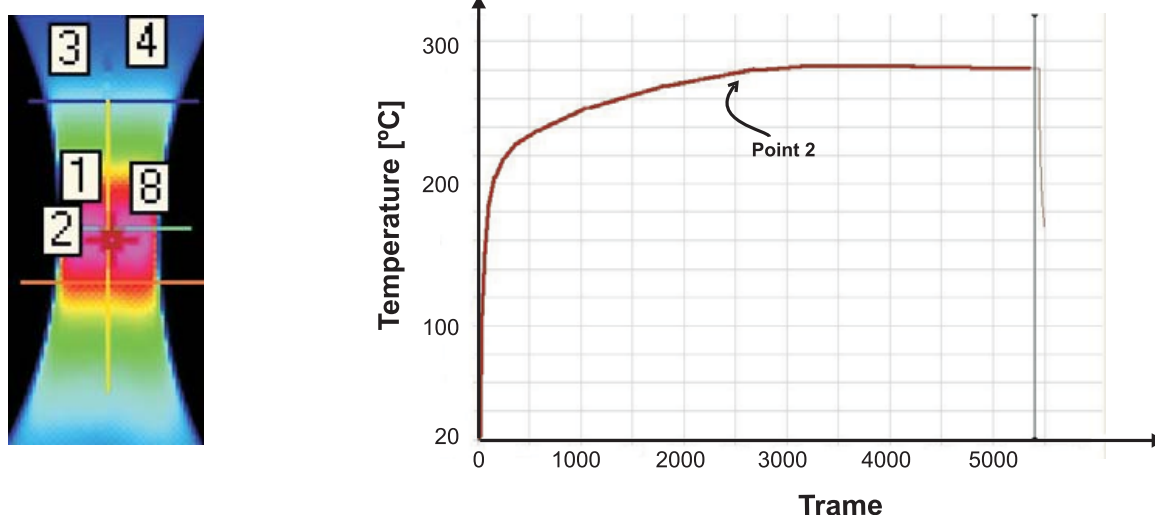


Figure 17: Temperature measured with an infra red camera.

7.2 S-N curve at 600°C

The stress life response of the material tested at 600°C is plotted in figure 18. In this case the S-N curve does not present an endurance limit, showing a continuously reduction in the fatigue stress with a strength lower than those of 20°C tests. The crack initiation in low cycle fatigue occurs in multiple sites on the surface. However, usually in gigacycle fatigue, the crack is initiated from an internal defect, inclusion, or pore. In this case, in specimens which failed at about 10^7 cycles, the crack started on the surface in a similar mode to room temperature tests. The rupture surface, in the middle of the specimen, presented an inclination of about 40° to the longitudinal axis. Figure 19(a) and 19(b) shows the fracture surface taken by an optical and SEM microscope respectively, with a crack initiated by a fish eye rupture mode in a specimen failed at 374×10^8 cycles and 315 MPa. This was the only specimen that failed from an internal inclusion. The diameter of the inclusion was $40\mu\text{m}$. Further examinations on crack initiation sites through SEM analysis indicated that the chemical composition of the inclusion was Nb, see figure 20. The Nb is a generator of carbides that stabilized the steel strength at high temperatures. It is usually used in austenitic steels of high strength at high temperatures and for this reason this element should not be avoided in the chemical composition of this steel.

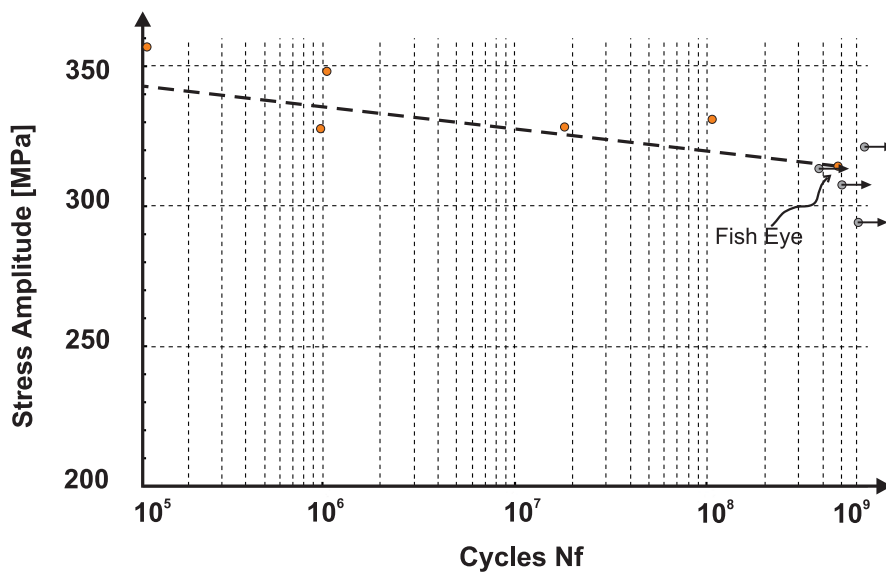
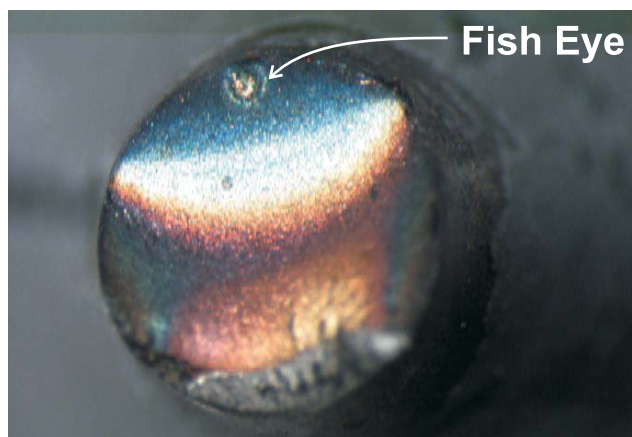
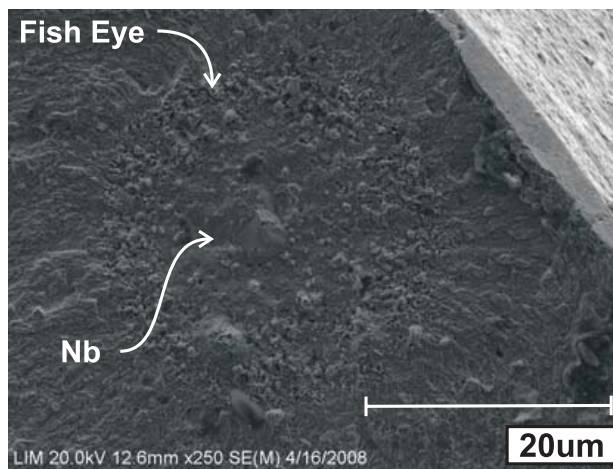


Figure 18: S-N curve at 600°C for the material analyzed.



(a) Fracture surface due to an inclusion.



(b) Zoom amplification at inclusion.

Figure 19: Fracture Surfaces in a specimen at 600°C.

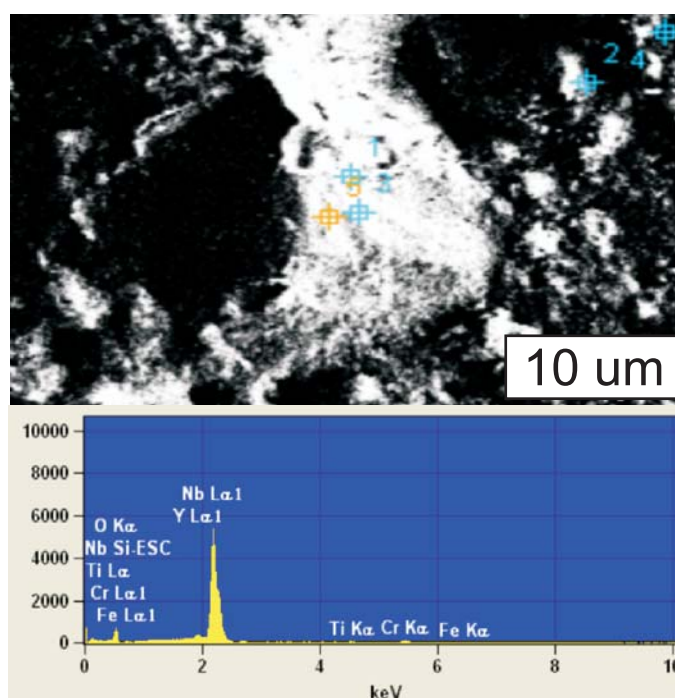


Figure 20: SEM spectrum, indicating that the inclusion is Nb.

7.3 S-N curve at 700°C

The stress life response of the material tested at 700°C is plotted in figure 21. The crack initiation was located in specimen surface and no interior cracks from inclusions were found. SEM figures 22(a), 22(b) show the fracture surface in a specimen failed at 345 MPa at 3×10^8 cycles for which the crack was initiated at the surface. Similarly to the rupture surfaces of 600°C specimens, they were in the middle of the specimen with an inclination of about 40° to the longitudinal axis.

The S-N plot shows a continuously decreasing stress-life response. In the range of 10^6 cycles, fatigue strength of the broken specimens is lower than those of the curve for 600°C, but at 10^9 cycles the stress is almost the same. This behavior could be explained two reason:

1. Oxidation phenomenon at the tip of the crack.

On the crack surface of the specimen tested at 600°C and 700°C oxidation was observed. At high temperature, crack propagation is accelerated, but the oxidation could decrease the propagation with a rate larger than due to the temperature.

2. Fish eye fracture mode.

It is important to note that the curve for 600°C presented only one type fish eye fracture mode with a low stress value, making that the fatigue curve, obtained from a least square method, decreases very fast until values nearby to specimens broken at 700°C.

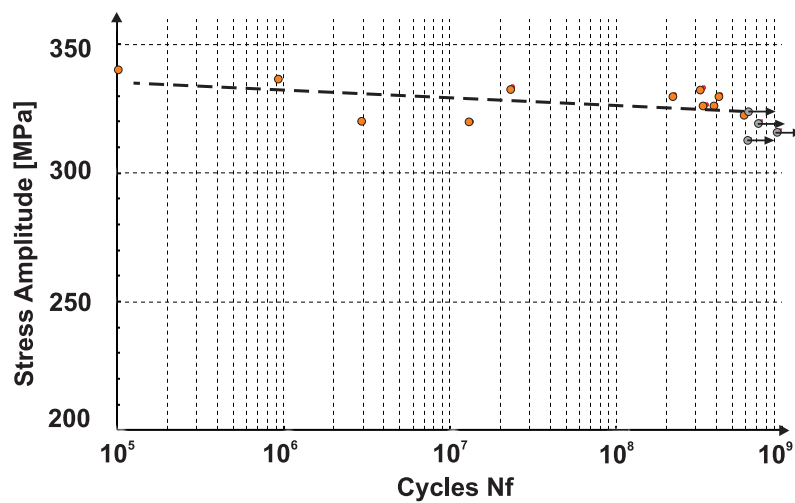
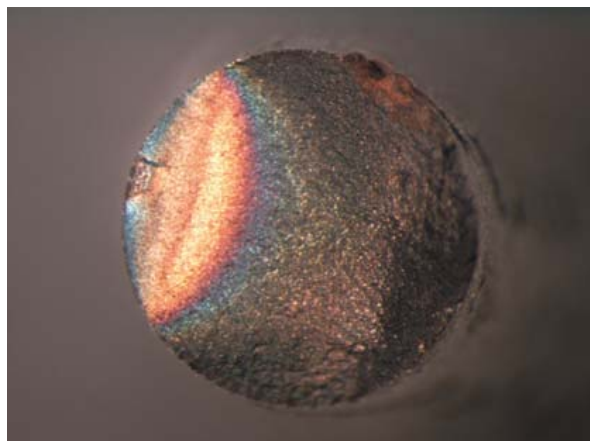
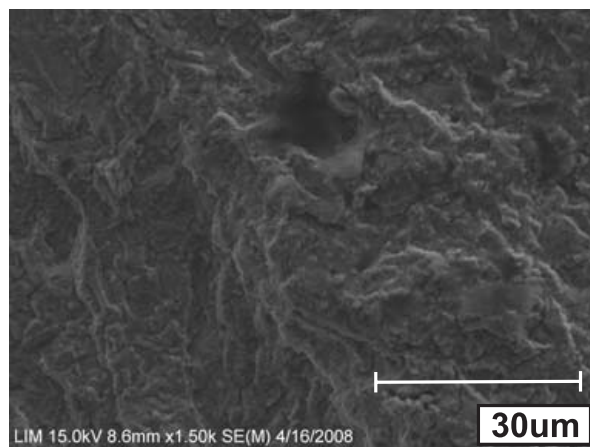


Figure 21: S-N curve at 700°C for the material analyzed.



(a) Fracture surface of specimen failed at 345MPa in 3×10^8 cycles at 700°C.



(b) Fracture surface of specimen failed at 345MPa in 3×10^8 cycles at 700°C.

Figure 22: Fracture Surfaces in a specimen at 700°C.

8 CONCLUSIONS

Ultrasonic fatigue technique was developed to determine fatigue behavior of austenitic steels in a range of 10^6 to 10^9 cycles under fully reverse loading at high and room temperature. The most important conclusions obtained are summarized below:

- The design of specimens for high temperature tests using FEM modal analysis, showed a good agreement with the experimental tests. When the specimen reached the desired temperature, *i.e.* 600°C or 700°C, natural frequency was close to 20kHz during ultrasonic fatigue test.
- Mechanical properties of austenitic steel subjected to high temperatures were identified based on numerical simulations and the measured resonant frequency of the specimens.
- At room temperature, the material presented an endurance limit in 341MPa. We concluded that a microstructural transformation from austenite to martensite was the main cause for premature failure.
- The 600°C S-N curve has shown a continuous decreasing stress-life response. Fatigue stress decreased about 34 MPa compared to the room temperature curve. In the specimens tested, the crack initiation was observed on the surface. SEM inspections showed that just one specimen failed by fish-eye rupture mode, being Nb the internal inclusion. In this sense, more experimental work is required to assess the influence of inclusions in fatigue for these type of steels.
- In a similar way, 600°C and 700°C curves showed continuous decreasing stress life-response. The crack initiation was identified on the surface in most failed specimens.
- The rupture surface in room temperature test was normal to the longitudinal axis of the specimen. Instead of at high temperatures the surface fracture presented a inclination of 40° to the principal stress. This characteristic is due to the creep phenomenon.

9 ACKNOWLEDGEMENTS

This work received financial support from Agencia Nacional de Promoción Científica y Técnica (ANPCyT) and the Programme AlBan, the European Union Programme of High Level Scholarships for Latin America, scholarship No.07D401463AR.

The first author thanks partnership of LEEE for their assistance, comments and discussions.

REFERENCES

- Bathias C., Drouillac L., and Le Francois P. How and why the fatigue s-n curve does not approach a horizontal asymptote. *International Journal of Fatigue*, 23:143–151, 2001.
- Bathias C. and Paris P. *Gigacycle Fatigue in Mechanical Practice*. Marcel Dekker, 2005.
- Bayraktar E., Garcias I., and C. B. Failure mechanisms of automotive metallic alloys in very high cycle fatigue range. *International Journal of Fatigue*, 28:1590–1602, 2006.
- C. B. Automated piezoelectric fatigue machine for severe environments. *ASTM STP 1411333333*, 4:3–15, 2002.
- C. B. Piezoelectric fatigue testing machine and devices. *International Journal of Fatigue*, 28:1438–1445, 2006.
- Curtis F. *High Frequency Induction Heating*. McGraw-Hill, 1950.

- Marines I., Dominguez G., Baudry G., Vittori J.F., Rathery S., and Doucet J.P. Ultrasonic fatigue tests on bearing steel aisi-sae 52100 at frequency of 20 and 30 khz. *Int. Mat. Rev.*, 44:1–36, 1999.
- Mayer H. Fatigue crack growth and threshold measurements at very high frequencies. *International Journal of Fatigue*, 25:1037–1046, 2003.
- SAMCEF. 2007. <http://www.samcef.com>.
- Shyam A., Torbet C., Jha S., Larsen J., Caton M., Szczepanski C., Pollock T., and Jones J. Development of ultrasonic fatigue for rapid, high temperature fatigue studies in turbine engine materials. *Superalloys 2004, TMS, Seven Springs, Pennsylvania, USA, 2004*, pages 259–268, 2004.
- Sun Z., Bathias C., and Baudry G. Fretting fatigue of 42crmo4 steel at ultrasonic frequency. *International Journal of Fatigue*, 23:449–453, 2001.
- Willertz L. Ultrasonic fatigue. *Int. Mat. Rev.*, 25:65–78, 1980.
- W.P M. Piezoelectronic crystal and their application in ultrasonics. page 161, 1950.
- Yi J., Torbet C., Feng Q., Pollock T., and Jones J. Ultrasonic fatigue of a single crystal ni-base superalloy at 1000. *Materials Science Engineering*, 443:142–149, 2007.
- Zettl B., Mayer H., Ede C., and Stanzl-Tschegg S. Very high cycle fatigue of normalized carbon steels. *International Journal of Fatigue*, 28:1583–1589, 2006.